Tectonophysics 898 (2025) 230642

Contents lists available at ScienceDirect

Tectonophysics

journal homepage: www.elsevier.com/locate/tecto

Seismicity, seismotectonics and historical earthquakes of the Northwestern Apennines, Italy: A reappraisal

E. Eva [a,*], G. Molli [b], F. Pettenati [c], S. Solarino [a]

[a] Istituto Nazionale di Geofisica e Vulcanologia, Osservatorio Nazionale Terremoti, Genoa, Italy
[b] Università di Pisa, Dipartimento Scienze della Terra, Pisa, Italy
[c] Istituto Nazionale di Oceanografia e di Geofisica Sperimentale, OGS, Trieste, Italy.

ARTICLE INFO

Keywords:
Northern Apennines
seismicity
focal mechanisms
geological structure
seismotectonics

ABSTRACT

The inner NW Apennines includes the Lunigiana region, which has been shaken by several strong (M > 6.0) earthquakes in the last millenium until the most recent 2013 Mw 5.1, Fivizzano earthquake. In this study we profit from more than 30 years of seismicity and an updated map of the faults to perform a seismotectonic analysis. In order to enlarge our study to the strongest events, we also compute the focal parameters of the 1834 and 1837 earthquakes applying the KF technique to macroseismic intensities. Our findings show that most of the seismicity in the study region is organized in clusters. The southern cluster is oriented nearly *E*-W and marks the border between the Lunigiana and Garfagnana grabens, NW of the Alpi Apuane. The northern cluster is less limited in size and number of events, and this masks the predominant apenninic NW-NNW orientation. NE of the Lunigiana graben, seismic events align along an apenninic direction as well. On the external side, earthquakes are almost perpendicular to the chain in an NEE-SWW orientation. Cross sections show the existence of three domains along the NE-SW direction. While the external and internal domains are well defined, the domain in between may represent the area in which switching from shortening to extension is ongoing. The processes occurring in this domain entail energies that are at times unleashed as considerable earthquakes, including the notable seismic event of 1834.

1. Introduction

The Northern Apennines formed as the result of Neogene subduction of the Adria continental crust below the Ligurian accretionary wedge (Carmignani and Kligfield, 1990; Gueguen et al., 1997; Faccenna et al., 2001; Le Breton et al., 2017). The latter is made up of oceanic basement slices and remnants of the Ligurian Tethys and the Ocean-Continent transition domain (Ligurian and sub- Ligurian units). The Ligurian prism was shaped during the pre-collisional stage of orogen development, and then, since Late Oligocene-early Miocene, superimposed to the Tuscan and Romagna–Umbria continental derived-cover and basement of the distal to proximal Adria plate (Fig. 1). The Neogene-to-recent tectonic evolution of the northern Apennines (NA hereafter) has been characterised by contractional tectonics in the external foreland domains, accompanied by extensional ones in the internal domain (Elter et al., 1975; Doglioni et al., 1998; Brozzetti et al., 2007; Eva et al., 2014).

The external foreland domain is characterised by two major fault systems (Royden et al., 1987; Benedetti et al., 2003; Butler et al., 2004): the Apennines Deformation Front (ADF, hereafter) and the Apennines Range Front (ARF, hereafter). The ADF and related fold-structures are buried beneath the Po whereas the ARF is well defined by the transition from gently dipping alluvial strata in the Po basin to uplifted bedrock in the Apennines. The topography of the range front represents a forward dipping limb of an anticline overlaying a steeply dipping blind reverse fault.

South-west of the orographic divide, the Tyrrhenian portion of the orogen is shaped by a variety of dominantly NW-SE and NNW-SEE trending normal fault systems (Fig. 1) which have extensional/transtensional kinematics documented by structural data and GPS-velocity field (Nirta et al., 2020; Molli et al., 2021; Devoti et al., 2008; Bennett et al., 2012).

In this inner domain the Lunigiana and Garfagnana basins are the northernmost of a series of early Pliocene to Quaternary, NW–SE-oriented, extensional grabens in the northern Apennines.

In this study, we focus on the Lunigiana area, which has been hit by

* Corresponding author.
E-mail address: elena.eva@ingv.it (E. Eva).

https://doi.org/10.1016/j.tecto.2025.230642
Received 1 August 2024; Received in revised form 24 January 2025; Accepted 25 January 2025
Available online 27 January 2025

large and destructive earthquakes in the last millennium, confirming that it is one of the most seismically active areas of the northern Apennines. In fact, more than 60 events of M > 4 shook the area in the period 1000–2022. The most important historical earthquakes occurred on 7 May 1481 (Maximum Intensity, hereafter Imax, VIII MCS; Mw ~ 5.6); 14 February 1834 (Imax IX MCS; Mw ~ 5.8); 11 April 1837 (Imax X MCS; Mw ~ 5.8); and 7 September 1920 (Imax X MCS; Mw ~ 6.5) (CPTI 15 catalogue, Rovida et al., 2022). Intensity data are primarily used to determine the locations of most of these earthquakes, except for a few occurrences from the twentieth century, among which the September 1920 earthquake, that have been investigated also using instrumental data by Solarino (2005). The strongest earthquakes are mostly located in the southern part of Lunigiana, close to the boundary between the Lunigiana and Garfagnana grabens. However, two M > 5 historical earthquakes were located at the northern edge of the Lunigiana, close to the Val di Taro, namely the 1545 and the 1834 seismic events. Previous research has largely overlooked historical earthquakes, primarily because of the difficulties in accurately assessing their locations and associated focal mechanisms. However, the present study introduces a specialized technique (Pettenati and Sirovich, 2003; Sirovich and Pettenati, 2004) that leverages macroseismic data to derive the focal mechanism.

In January and June 2013, the sector under study was hit by several earthquakes, the largest of which were the Mw 5.1 located 7 km NE of Carrara and the Mw 4.8 located 7 km NE of Castelnuovo di Garfagnana. These events are the largest to have been recorded by instruments in this region. Their analysis holds significant importance for advancing the comprehension of the seismotectonics within this area of the Northwestern Apennines. In the present study, the recent update of the seismic catalogue, which now includes data up to 2022, offers a more detailed

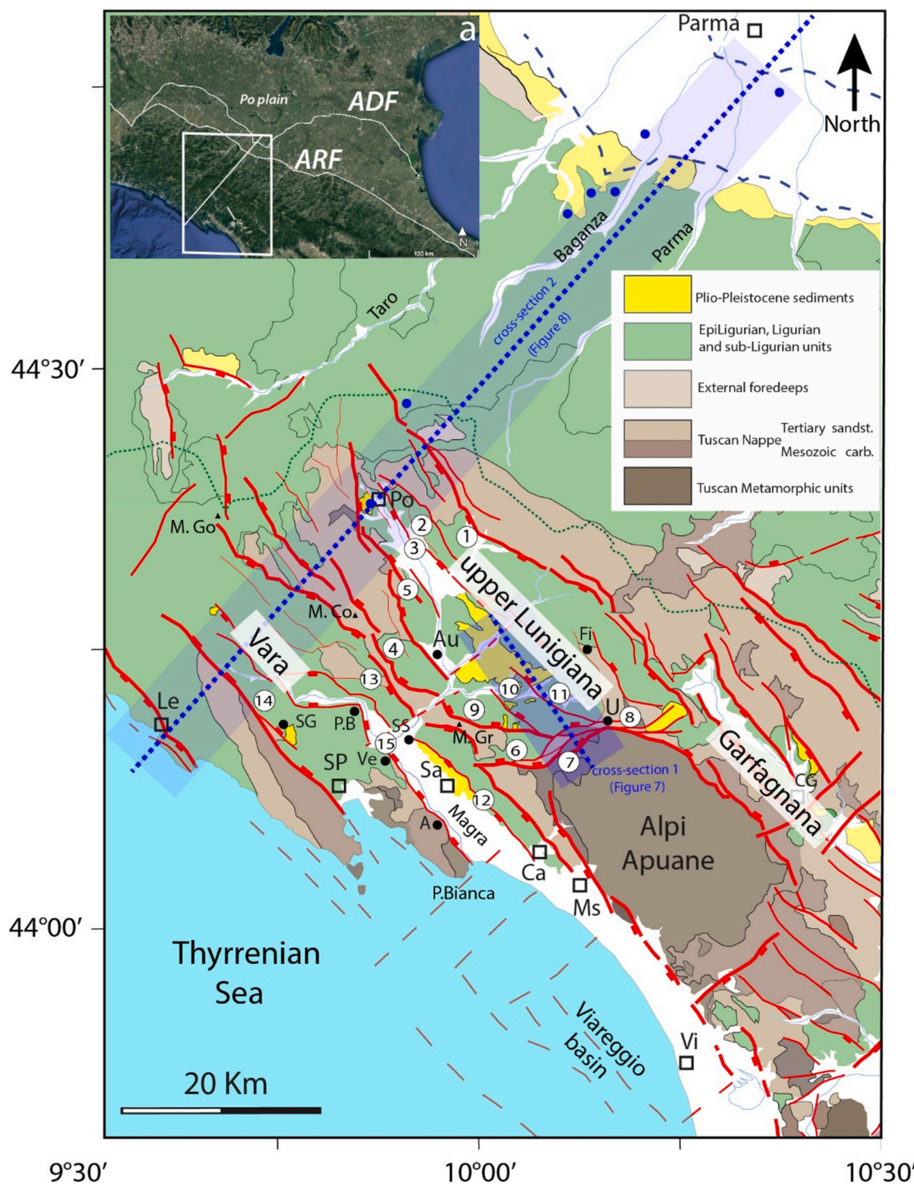

Fig. 1. Geological map of the area under study. Blue dashed lines indicate the traces of the cross-sections 1 and 2; green dashed line: orographic divide; Fault systems in the text: (1) Groppodalosio–Compione–Comano; (2) Arzengio–Bagnone; (3) Mocrone–Licciana; (4) Coloretta–Parana–Podenzana; (5) Arzelato–Mulazzo–Tresana–Aulla; (6) Fosdinovo fault; (7) Tenerano–Marciaso fault; (8) Aiola–Equi Terme; (9) Ponzanello–Tendola; (10) Gorasco; (11) Olivola–Soliera; (12) Sarzana–Carrara; (13) Mt. Grosso-Mt. Cornoviglio-M.Vruga; (14) La Spezia; (15) Piano Battolla–Vezzano– Ameglia. M.Go: Monte Gottero; M.*Co* (Monte Cornoviglio); M.*Gr*: Monte Grosso. M.Go: Monte Gottero; M.*Co*: M.Cornovoglio; M. *Gr*: Monte Grosso. Le: Levanto; Po: Pontremoli; Au: Aulla; Fi: Fivizzano; U: Ugliancaldo; SP: La Spezia; SG: Sesta Godano; P·B: Piano Battolla; SS Santo Stefano di Magra; Ve: Vezzano; SA: Sarzana; Ca: Carrara; Ms.: Massa; Vi: Viareggio; CG: Castelnuovo Garfagnana. (For interpretation of the references to colour in this figure legend, the reader is referred to the web version of this article.)

insight into the seismic activity and seismotectonic characteristics of the area.

Through the integration of the aforementioned seismological studies and a newly developed map of the fault network, this study presents a novel interpretation of the seismotectonics of the NW Apennines, addressing, to some extent, the constraints identified in earlier studies. The approach aims to enhance our understanding of historical seismic events over the past two centuries, thereby aiding in the interpretation and possible scenario of future occurrences.

2. Tectonic setting of the inner Northwest Apennines

West of the orographic divide the inner Northwest Apennines is characterised by two main graben systems hosting the course of the Magra and Vara rivers (Fig. 1). The two grabens, the upper Lunigiana and the Vara-Lower Lunigiana, include remnants of diachronous South to North, Late Pliocene (Villafranchian)- to early Pleistocene fluvio-lacustrine to fluvial continental stratigraphic sequences (Bernini and Papani, 2002; Bonini et al., 2016; Nirta et al., 2020; Molli et al., 2021).

The upper Lunigiana is shaped by a c.40-km long NW-SE-oriented northward-tapering system of extensional structures. To the east, the west-dipping faults are arranged in 3 subparallel, NW-trending, closely spaced (a few km) faults i.e. the Groppodalosio–Compione–Comano, the Arzengio–Bagnone, and the Mocrone–Licciana strands (Fig. 1). To the west the antithetic NE-dipping faults include two main strands: the Coloretta–Parana–Podenzana–Tendola and the Arzela-to–Mulazzo–Tresana–Aulla faults (Bernini and Papani, 2002; Di Naccio et al., 2013; Piccardi et al., 2019; Nirta et al., 2020; Molli et al., 2021).

The upper Lunigiana southward ends against the Alpi Apuane horst (Fig. 1) forming a kilometre-wide domain linkage zone with the south-easternmost Garfagnana graben (Brozzetti et al., 2007; Eva et al., 2014; Molli et al., 2016). On the surface, the linkage zone is formed by the North Apuane Fault System (NAF) which extends over a length of more than 30 km and is divided into three connected, ~10 km long faults namely from West to East, the ~E–W trending Fosdinovo fault, the central ~NE-SW trending Tenerano–Marciaso fault, and the ~E–W trending, Aiola–Equi Terme fault. The NAF shows a total vertical slip of c. 3 km. The overall architecture of the NAF is completed by secondary splay faults such as the Ponzanello–Tendola, Gorasco and Olivola–Soliera faults which form a large horsetail at the western termination of the NAF system, in consequence of the right-lateral component of slip (Fig. 1).

West of the upper Lunigiana, the Vara Valley–lower Lunigiana grabens host the Vara and the lower course of the Magra river. The western promontories of La Spezia and the Pta. Bianca bound west the graben that to the east is defined by the Mt. Gottero-Mt.Cornoviglio- Mt. Grosso horst. To the east, the major west-dipping Sarzana–Carrara fault, the northernmost part of the West Apuane Fault System, extends over ~25 km from Carrara to S. Stefano di Magra, where it steps to the right to continue through the Mt. Grosso-Mt. Cornoviglio-M. Vruga fault (Raggi, 1985; Molli et al., 2021). From the step toward the northwest, the Sarzana–Carrara fault splays into a network of curved normal faults, forming a sort of horsetail that suggests a left-lateral component of slip on the main NW-trending Sarzana–Carrara fault, in addition to its dominant normal one. To the west of the graben, the east-dipping, NW-trending bounding normal fault system includes La Spezia fault, about 20 km long, and the Piano Battolla–Vezzano– Ameglia fault on the eastern side of the Punta Bianca promontory. With a total length of about 40 km, the Piano Battolla–Vezzano–Ameglia fault bends counterclockwise in its northern section, likely to connect to the La Spezia fault.

3. Instrumental seismicity

3.1. Seismicity of the Northwestern Apennines

The seismicity of the area has been investigated in several works (Eva et al., 1978; Solarino et al., 2002a, 2002b; Eva et al., 2005; Eva et al., 2014). The present study undertakes a comprehensive analysis of the research conducted by Eva et al. (2014) by leveraging an enriched database incorporating supplementary events occurring between 2012 and 2022 in the quadrangle of latitude 44.0°-44.8° and longitude 9.5°-10.5°. Waveforms from 60 seismic broadband stations located within approximately 120 km from the study area's center were retrieved from the EIDA database (Strollo et al., 2021). Data were manually analysed for phase picking and selected upon criteria of at least 8 (P + S) phase picks and a gap of 180°, summing up to a database of 2574 events. Earthquakes were initially located using Hypoellipse (Lahr, 1999), a software application used for standard positioning that delivers a satisfactory compromise among the accuracy of location, the time needed to determine hypocenters, and the computational resources required. Given that locations determined by Hypoellipse may not be suitable for sophisticated seismotectonic applications (as noted in Eva et al., 2020, and Eva et al., 2023), more precise locations have been obtained through HypoDD (Waldhauser and Ellsworth, 2000). This high-precision location algorithm utilizes the double difference method for events that are spatially correlated and recorded at the same stations.

3.2. HypoDD

HypoDD takes advantage of the fact that if the hypocentral separation between two earthquakes is small compared to the event-station distance and the length scale of velocity heterogeneity, then the ray paths between the source region and a common station are similar along almost the entire ray path (Frechet, 1985; Got et al., 1994). The difference in travel times for two events observed at one station can be attributed to the spatial offset between the events. This difference is then the input of the DD procedure. In this way, the residual between observed and calculated travel-time difference (or double-difference) between two events at a common station are related to adjustments in the relative position of the hypocenters and origin times through the partial derivatives of the travel times for each event with respect to the unknown. Solutions are found by iteratively adjusting the vector difference between nearby hypocentral pairs, with the locations and partial derivatives being updated after each iteration.

HypoDD uses input data from phase picks or waveform cross correlations. These data have a different accuracy which depends on the way they are obtained. Phase picks are the results of the recognition of phase arrival times performed by an operator or an automated procedure. Their reliability depends on several factors, including the experience of the operator. Cross correlation data are instead computed by an algorithm and do not suffer, or at least less, of subjectivity. Moreover, a threshold can be fixed in order to get rid of low quality correlations. However, cross-correlation is time demanding and can be performed only if waveforms are available. In our case we used both phase picks data and waveform cross-correlations. For cross-correlation, waveforms were cut 10 s before the origin time and 50 s after the origin time. Waveforms were bandpass filtered [1–9 Hz] and processed for similarities in the time domain using samples of 2 s for P waves and 3 s for S waves (Schaff, 2004). The cross-correlation threshold was set to 70 %.

The database created is inherently hybrid due to its composition of data with varying quality. This characteristic is largely a result of the difficulties encountered in cross-correlating seismic events that have been recorded with differing parameters (for instance, sampling rates) or by stations that are no longer operational. However, it is essential to consider a broad observation period to adequately capture the seismicity of the area under study, thus encompassing older instrumental earthquakes. Despite these challenges, the correlation between the events analysed via cross-correlation and those processed through conventional methods is not so unfavorable. In fact, the seismic phases validated by cross-correlation account for approximately 35 % of the total.

Adding new data like in the present case, namely the 2012 to 2022 earthquakes, needs an exploration for new “earthquake pairs” on the resulting database. We built a network of links between events to form a chain of linked event pairs. We calculated travel time differences between events after choosing a maximum of 15 neighbours per event within a distance of 20 km. Event pairs with at least 8 observations were retained, since the number of unknowns for an event pair is 8, and a maximum number of observations in each event pair was set equal to 15.

The locations of closely spaced events typically exhibit minimal dependence on the velocity model; however, the use of an incorrect velocity model may have repercussions on the results obtained from the HypoDD runs (Wolfe, 2002; Michelini and Lomax, 2004). We then computed a 1-D model using the code VELEST (Kissling, 1988), which provides a layered velocity model and the relative station corrections by inverting a selection of reliable phase picks for earthquakes occurring in the area where the model is searched for. VELEST is a trial and error procedure: several models are computed changing the input parameters. The model that best minimizes the RMSs of the input data is then chosen as the reference, or Minimum, 1-D model. In our case, a subset of about 1000 seismic events were inverted in VELEST.

3.3. Results and comparison between standard and HypoDD locations

The HypoDD code refines clustering according to a selected maximum distance between connected pairs. In each run, we progressively decreased the maximum distance between connected pairs. The application of HypoDD ensures greater accuracy in the location at the expense of a diminution of located earthquakes. The final number of events dropped to 1673 compared to the initial 2574.

Fig. 2 shows the preliminary hypocentral distribution of the data set used in this work as obtained with the “standard” Hypo technique on the left side and relocated by HypoDD on the right side. The comparison of the locations in the two panels shows that the structural details, such as the positioning of active fault planes, are clearly highlighted when HypoDD is used, although this comes at the cost of a reduced number of relocated earthquakes in comparison to standard locations. The relationship between seismicity and faults will be highlighted in the next paragraphs, where geo-seismic cross sections will be described. Most of the seismicity is located NW of the Alpi Apuane. Seismic events are

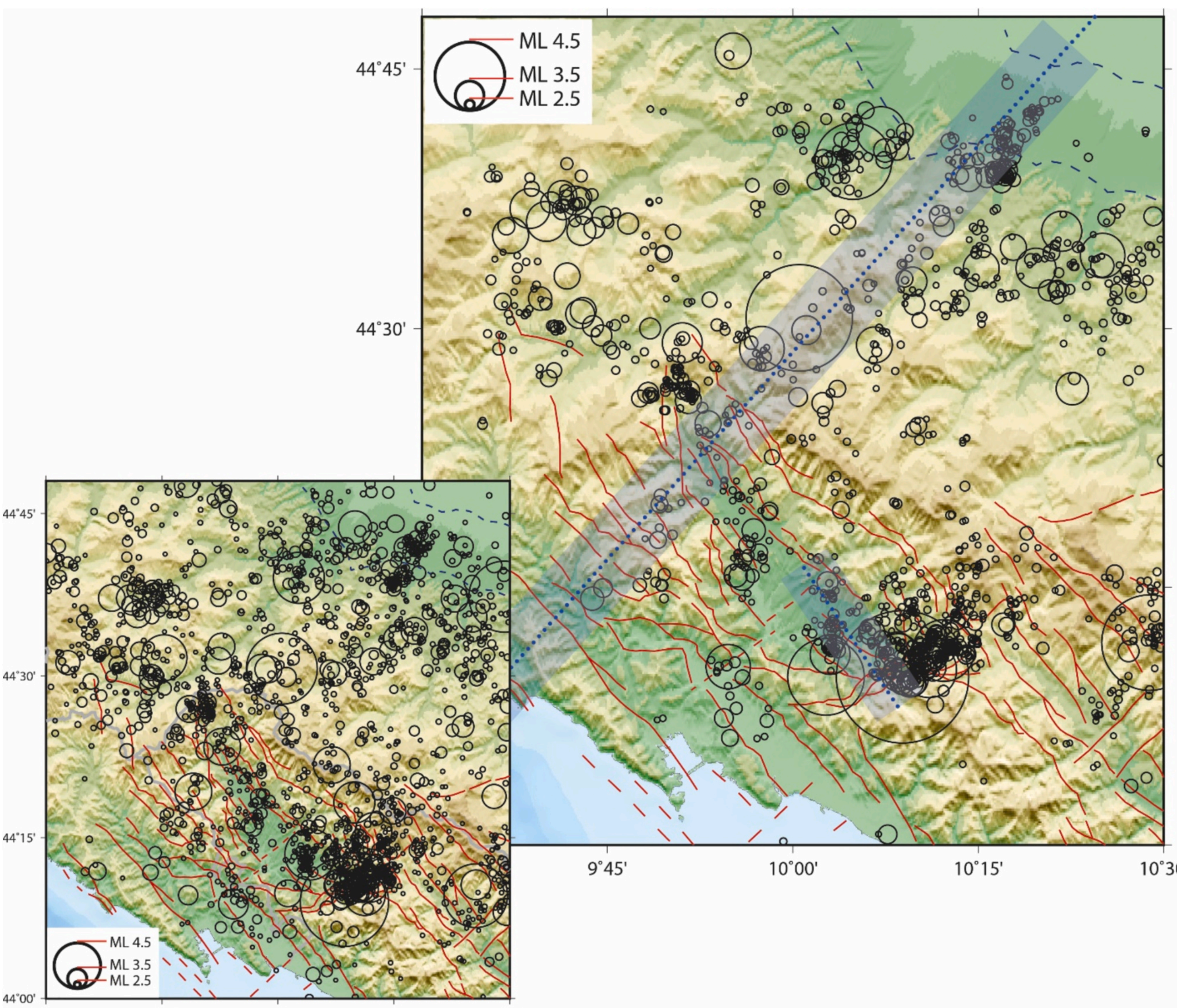

Fig. 2. Left bottom panel: preliminary hypocentral distribution of the data set used in this work as obtained with the “standard” Hypo (Lahr, 1999) technique. Right: Relocated seismicity by HYPODD (Waldhauser and Ellsworth, 2000). In red, in both pictures, the network of fault systems of the inner NW Apennines are shown (Molli et al., 2021). (For interpretation of the references to colour in this figure legend, the reader is referred to the web version of this article.)

diffuse and bordering the Lunigiana graben, although dense clusters of epicentres mark the northern and southern terminations. The southern cluster, which includes the 2013 events, is oriented nearly *E*-W and marks the border between the Lunigiana and Garfagnana grabens. South of this cluster, a strong reduction of seismicity is observed, and the locations are shifted to the eastern sector. The northern cluster is less limited in size and number of events, and this masks the predominant apenninic NW-NNW orientation. NW of the Lunigiana graben, the seismic events align along an apenninic direction as well. On the external side, earthquakes are almost perpendicular to the chain in a NEE-SWW orientation.

This is particularly evident at the N-E termination of the Taro and Enza valleys and along the Parma valley. South of it, an aseismic area extends until the border of the northern Garfagnana graben. A smaller aseismic area, bordered by two domains with anti-apenninic orientation, is located in the quadrangle right NW of the 2013 events.

4. Focal mechanisms for historical earthquakes

4.1. Intensity data

Historical seismicity is seldom used in seismotectonic interpretation since historical earthquakes 1) are often not adequately constrained by intensity data (Solarino, 2005), 2) do not provide the hypocentral depth 3) are not considered useful for the computation of focal mechanisms. However, macroseismic intensity patterns not only may provide the location for pre-instrumental earthquakes but, in some cases, are suitable for computing additional information. In this study, we applied the Kinematic Function *KF* (Sirovich, 1996; Pettenati and Sirovich, 2003) that allows inferring quantitative hypotheses about the geometry and kinematics of the seismic source using intensity data to the 1834 and 1837 events to discuss their locations and focal mechanisms in the light of a reappraised seismotectonic interpretation.

We had two diverse datasets available for the inversion process. One is the DBMI15 catalogue (Locati et al., 2022) and the other is a review of macroseismic data published by Moroni, 2001. The two datasets differ significantly, especially at the higher intensities. Since there is no objective way to determine the most reliable set beforehand, we chose to invert both datasets.

For the Mw 5.94 earthquake of 11 April 1837, the CPTI15 dataset (Fig. 3a) consists of a cluster of intensities in the epicentral area and some data below the V degree in the NE area of the Emilian Apennines (not shown in Fig. 3a). All intensities fall in the range between 5 and 100 km from the macroseismic epicentre, the useful distance range for the KF inversion. However, we only inverted data clusters VII to X near the epicentre, as the elongated distribution in the north-south direction could influence the results. The maximum intensity I_0 X (Ugliancaldo) is surrounded, at distances even less than 5 km, by intensities VIII and VII. Due to the lack of intensities in between (X or IX) to corroborate that value, it is speculated that the intensity X is due to a local effect or, as remarked by Moroni (2001), to the high vulnerability of buildings. The strong variation in intensity between the maximum value and those that follow cannot be modelled by the KF model; the gap creates a disturbance in the result due to the strong influence that the clusters of the intensities VIII and VII have on the epicentral zone. The Moroni (2001) dataset (Fig. 3b) shows a maximum intensity I_0 (Ugliancaldo) equal to IX-X and is surrounded by intensity from VIII to VI. It is important to note that the DBMI15 includes a larger volume of data compared to the Moroni dataset. Generally, it is advisable to choose the dataset with the higher intensity count when two options are available. However, in this particular case, the Moroni dataset shows a more uniform distribution, which should be taken into consideration.

The DBMI15 dataset includes a greater amount of intensity data also for the Mw 5.96 earthquake that occurred on 14 February 1834, featuring 104 entries compared to the 89 included in the Moroni's dataset. The two databases (Fig. 4 a and b) share a common issue in that they show a gap in the ENE sector in correspondence with the former Duchy of Modena, due to scarce interest from the Duchy of Modena for his distant enclaves, more than a lack of damage at those places (Moroni et al., 1993). The earthquake is not reported in the documents of such authorities and the intensities for that area were not included in any data review. Moreover, the DBMI15 reports two intensities IX very distant from each other. On the other hand, the Moroni dataset slightly underestimates the intensities compared to the DBM15 data, but the overall distribution looks more homogeneous.

It is important to note that the uncertainties associated with attributing intensities are frequently addressed by employing half degrees (for instance, III-IV indicates that the damage or effect lies between the expectations for the two respective degrees). We have opted for a more conservative approach by rounding down the intermediate degrees (for example, VI-VII is adjusted to VI) across all datasets.

4.2. The KF method

The KF algorithm computes the location, seismic moment and focal parameters of historical earthquakes using intensity data; the quality of the solution is estimated by a misfit value. The technique has been applied to numerous datasets, and a short summary is presented in the

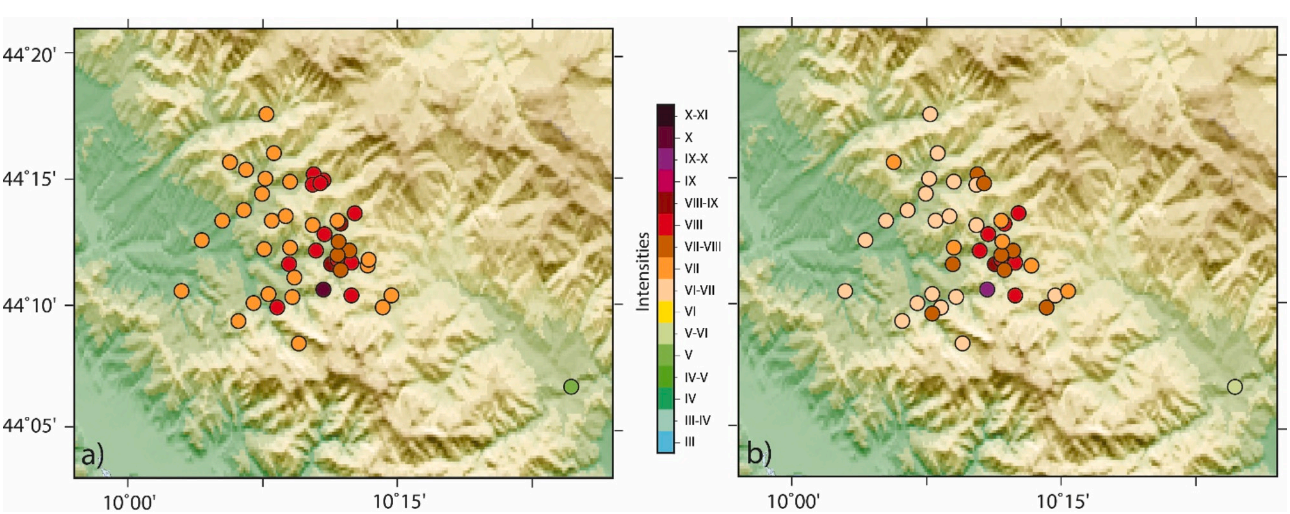

Fig. 3. Macroseismic intensities used for the KF inversion of the 1837 event: a) intensities from the DBMI15 catalogue (Locati et al., 2022); b) intensities from Moroni catalogue (Moroni, 2001).

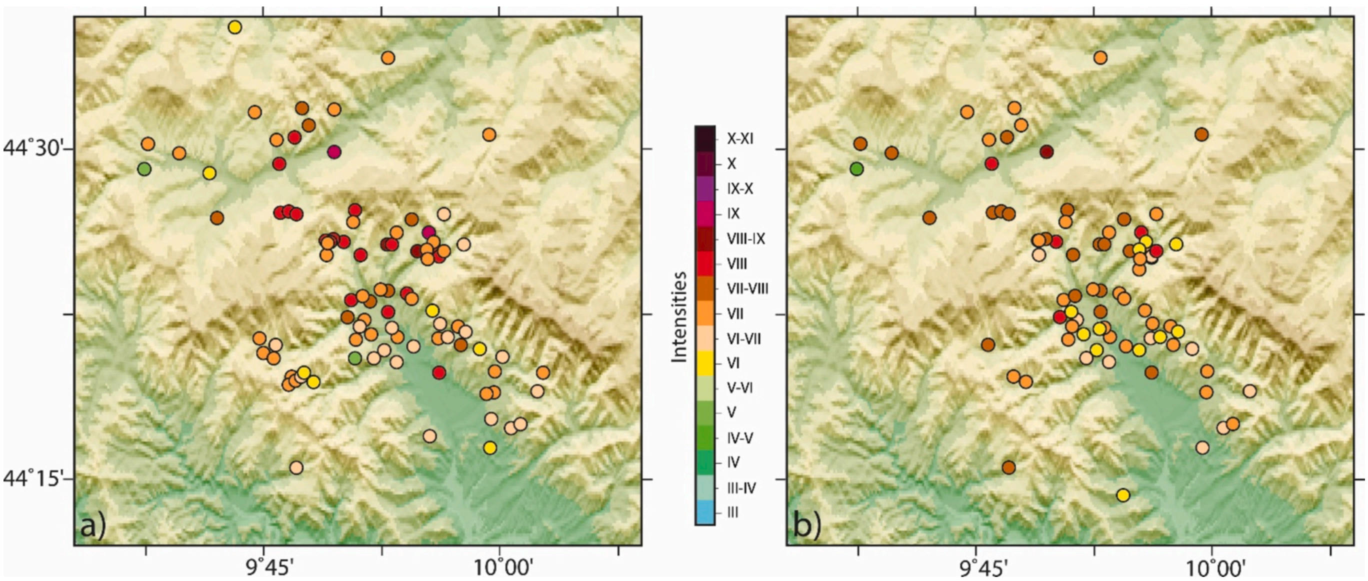

Fig. 4. Macroseismic intensities used for the KF inversion of the 1834 event: a) intensities from DBMI15 catalogue (Locati et al., 2022); b) intensities from Moroni catalogue (Moroni, 2001).

lines that follow.

KF is defined as the contribution of a source dislocation point propagating along a horizontal line, on a rupture plane of unit width at depth H and distance l from the nucleation point, to the displacement-related ground motion at the receiver point P on the surface.

$$KF(P,l) = \frac{R(P,l)}{D\left(P,l\right)\left[1-\left(\frac{V_r}{V_s}\right)\cos\theta(P,l)\right]}$$

KF considers body-wave and $R(P,l)$ is the radiation pattern of S-waves (Aki and Richards, 2002), while $D(P,l)$ is the distance between the source and the receiver P and $\theta(P,l)$ is the angle between the ray reaching P and the direction of the rupture propagation. To put in short, on the denominator is the geometrical spreading of the waves and the other term is the directivity. *KF* uses as a propagation medium an elastic half-space in the distance range of about 5 to 100 km from the source, and wavelengths shorter than the shortest distance between observer and source. *KF* is consistent with the asymptotic approximation (Bernard and Madariaga, 1984). In the asymptotic assumption, only the far-field term of the impulse response (Green's function) in the representation theorem is used. Roughly speaking, the limit of 100 km is the range of only direct body-waves, since the KF function uses only a homogeneous elastic half-space. The *KF* model uses 11 source parameters adopting the convention of the positive direction of the strike ranging from 0° to 360°, with the fault plane dipping to the right. According to this, rake angles between 0° and 179° indicate faults with reverse (compressive) components, while from 180° to 359° indicate normal (distensive) components. In our convention, the total length of the rupture is the sum of the absolute values of the parts along-strike (considered positive L+) and antistrike (negative L-). The same goes for the Mach number (Mach+, and Mach-). The length is calibrated to lie within the range of the empirical relationship M versus RLD (subsurface Rupture Length, Wells and Coppersmith, 1994) for all types of faults. The twelfth parameter is the seismic moment Mo, which is used in the computation to convert the values of *KF* into pseudo-intensities I_{calc} by the semi-empirical data-fitting function in Sirovich et al., 2001 and formula 2 in Pettenati and Sirovich, 2003. To perform this kind of inversion, we need a model of the source radiation. The model should be as simple as possible, see for example Sirovich et al. (2009).

Due to the high computational requirements related to CPU and time, we have decided to adopt a stepwise inversion. This approach is practical for our needs, particularly as our datasets are not extensive. This approach allows for enhanced control over the inversion process compared to the Niching Genetic Algorithm (*NGA*) used in other works (Gentile et al., 2004; Pettenati et al., 2017, 2018). Thus, we used a system of six nested loops to run all the parameters for the different earthquakes. One loop is for the Mo, which converts the *KF* values calculated with the parameter combinations of the previous loops into pseudo-intensities. When using six parameters for the six loops, for the other five parameters we choose a fixed value consistent with trend of inversion. With different runs of KF inversions, we can use sources with all parameter combinations.

Since the function KF is too complex to use a linear method as the Hessian matrix, we used the randomization by the Monte Carlo technique as performed in other papers (Pettenati and Sirovich, 2007; Pettenati et al., 2017, 2018). We build a random number N (50 < N < 100) of artificial intensity datasets. All sites were then assigned a new *I*, and each artificial set was assembled under the following conditions: i) The artificial values must lie within the I–XI limits. ii) Assuming a normal distribution centred on the observed *I*obs value with a standard deviation of one degree, the maximum difference between the artificial value and *I*obs must be two degrees. iii). An exception was allowed because the boundary between degrees V and VI (i.e., between non damage and damage) is particularly reliable: intensities less than V could not exceed VI, and intensities greater than VI could not be less than V. In setting these limits, an average of 37 % of the *I*obs was substituted for the two sets. In Tables 1 and 2, two standard deviations were used as 95 % probability errors.

4.3. Results

As previously noted, we carried out the inversion on both datasets. To improve our understanding of the differences between DBMI15 and Moroni, we display the Voronoi polygons (Okabe et al., 2000; Pettenati et al., 1999). For instance Moroni (2001) (Fig. 5) contains a data intensity for the 1837 earthquake on the western side, which completes the azimuthal distribution; this data point is lacking in the DBMI15 dataset. This difference is significant for the inversion results.

The results of the inversions for the 1837 earthquake are shown in Table 1. The left column shows the result of the DBMI5 dataset made of 46 sites, while the other two columns show the results of the inversion of the Moroni dataset (42 sites). The inversion method KF, as discussed in

Table 1
Complete results of the inversion for the 1837 earthquake using different datasets.

Parameter	CPTI15 46 intensities	Moroni 42 intensities solution 1	Moroni 42 intensities solution 2
Lon. E [°]	10.23 ± 0.02	10.33 ± 0.03	10.29 ± 0.03
Lat. N [°]	44.25 ± 0.01	44.23 ± 0.05	44.21 ± 0.06
Strike [°]	126 ± 10	106 ± 14	296 ± 25
Dip [°]	34 ± 1	58 ± 14	46 ± 11
Rake [°](*)	266 ± 14 [−94]	265 ± 8 [−95]	288 ± 10 [−72]
Depth [km]	18 ± 1	9 ± 2	10 ± 3
L + [km]	9 ± 5	5 ± 1	5 ± 2
L - [km]	3 ± 2	6 ± 1	4 ± 2
Mach +	0.72 ± 0.03	0.62 ± 0.25	0.70 ± 0.07
Mach -	0.68 ± 0.04	0.60 ± 0.06	−0.65 ± 0.25
S-wave vel. [km s^{-1}]	3.72 ± 0.05	3.74 ± 0.20	3.70 ± 0.25
M_0 [N m] 10^{17} (M)	8.0 ± 1.5 (5.9)	0.26 ± 1.0 (5.57)	0.46 ± 0.08 (5.74)
Misfit -	8	15	15

(*) KF method cannot distinguish between a rake and the symmetric rake (±180. In the table, we have reported the rake of a distensive mechanism discriminated by tectonic information (see text) in the KF and Aki (in square brackets) convention.

Table 2
Complete results of the inversion for the 1834 earthquake using different datasets.

Parameter	CPTI15 104 intensities	Moroni 89 intensities
Lat. N [°]	44.49 ± 0.11	44.44 ± 0.07
Lon. E [°]	9.84 ± 0.08	9.87 ± 0.15
Strike [°]	116 ± 20	145 ± 10
Dip [°]	33 ± 13	48 ± 3
Rake [°](*)	228 ± 30 [−132]	246 ± 20 [−114]
Depth [km]	12 ± 6	15 ± 5
L + [km]	6 ± 1	6 ± 1
L - [km]	4 ± 2	6 ± 1
Mach +	0.80 ± 0.20	0.67 ± 0.05
Mach -	0.79 ± 0.20	0.67 ± 0.05
S-wave vel. [km s^{-1}]	3.66 ± 0.20	3.67 ± 0.13
M_0 [N m] 10^{17} (M)	0.6 ± 0.2 (5.2)	0.88 ± 0.15 (5.92)
Misfit -	42	30

(*) See Table 1.

following lines, provides more than one solution. In some cases, the same mechanism, with fault and auxiliary planes switched, is computed for different solutions (Sirovich and Pettenati, 2004). In Table 1 the two solutions using the Moroni dataset have the same misfit (15) and yield values of strike, dip, rake compatible with the same focal solution. (106, 58, 265 in one case and 296, 46, 288 in the other). This is a good result for a dataset with few data and non-optimal distribution. It is noteworthy that the misfit computed with the DBM15 dataset is about half that of Moroni's, despite the former having only four additional sites. However, we consider the results from Moroni's dataset to be more reliable due to its more homogeneous spatial distribution, as previously discussed. We prefer solution 2, as it is better aligned with the distribution of the macroseismic data and its magnitude is consistent with the maximum intensity observed.

Regarding the 1834 data, we also performed the inversion of both available datasets, and the results are summarized in Table 2. Since the misfit from the inversion of the DBMI15 database is higher than that of the Moroni, we have selected Moroni's dataset as the preferred solution also taking into account its homogeneity, as previously discussed.

It must be kept in mind that the *KF* method uses intensities, which are expressions of the radiation pattern but do not carry information about the polarity. Therefore, the algorithm is not able to distinguish between mechanisms that differ in the rake angle by 180°. As a consequence, for example in the case of a pure dip-slip, the KF cannot discriminate whether the kinematics is distensive or compressive (Sirovich and Pettenati, 2004). This ambiguity can only be resolved by instrumental records, additional tectonic information or suited evidence. The solutions we have chosen for the 1834 and 1837 earthquakes are both dip slip with a slight oblique component and nodal planes almost EW (anti apenninic) oriented for the 1837 and NW apenninic oriented for the 1834; however, due to the intrinsic limitation of the KF method, we could not decide which type of fault (normal or thrust) generated the two earthquakes. We thus profited from a comprehensive database of focal mechanisms to clear the ambiguity. It has been obtained by integrating focal solutions derived from Eva et al. (2014) for the years 1995 to 2012 with additional focal mechanisms from 2012 to 2023. All were computed using the first onset methodology through the FPFIT software (Reasenberg and Oppenheimer, 1985), targeting events with at least 20 polarities and adequate azimuthal station coverage (gap <70°). To all events the Ml magnitude has been assigned except when the Mw was available.

The focal mechanisms in the area under study (Fig. 6) show a different trend above and below 17 km depth; in particular in the layer shallower than 17 km only pure strike slip and transtensional mechanisms are located, while at greater depth the transpressional component prevails. In such a frame, both focal mechanisms of the 1834 and 1837 earthquakes, having a depth of 15 and 10 km respectively, belong to the extensional domain (Fig. 6). It is noteworthy that the mechanism of the 1837 event resembles that of June 21, 2013.

5. Geological and seismological cross sections

With the aim to shed some light on the relationship between the seismicity and structural architecture of the studied portion of the NA, we focus on two cross sections located in the area affected by the historical 1834, 1837 and 2013 earthquakes. The seismicity and focal mechanisms obtained in this study have been superimposed on geological sections, one in a NW-SE direction at the southernmost termination of Lunigiana (section 1, Fig. 7) and the other at regional scale in an NE-SW direction from Levanto across the Baganza Valley to the Po plain (section 2, Fig. 8). Seismic cross-sections have a width of 6 km (3 km per side with respect to the center) and 8 km respectively (see Figs. 2 and 6). In addition, cross-section 2 is completed at depth by the tomographic model by Scafidi and Solarino (2012). The tomographic images provide insights on the velocity structure and the geometry of the Thyrrenian and Adriatic Mohos which, as confirmed by several studies (e.g. Diehl et al., 2009; Handy et al., 2010; Di Stefano et al., 2011; Spada et al., 2013; Di Stefano and Ciaccio, 2014), lie at about 25–30 and 35–40 km depth respectively.

The two cross-sections derived from commercial 2-D seismic reflection profiles made available by ENI S.p.A. The cross-sections were already interpreted, from the structural point of view, in Camurri (2000); Camurri et al. (2001); Argnani et al. (2003); Di Naccio et al. (2013), Carlini et al. (2013); Turrini et al. (2014); Turrini et al. (2016) and, more recently, Livani et al. (2018); Molli et al. (2018). The seismic reflectors and subsurface geology have been validated by stratigraphies of boreholes (Pontremoli, Lama dei Cerri, Vigatto, Felino1, Collecchio, Parma 1 wells) located close to the traces of the seismic reflection lines. Stratigraphies obtained from well logs are freely available and downloadable from the ViDEPI Project database (http://unmig.sviluppoeconomico.gov.it/videpi/).

5.1. Cross-section 1

The cross-section 1 (Fig. 7) is traced across the North Apuane Fault (Brozzetti et al., 2007; Di Naccio, 2009; Stramondo et al., 2014; Pezzo et al., 2014; Molli et al., 2016) which is part of the fault system defining the linkage zone between Lunigiana and Garfagnana grabens (Eva et al., 2014; Nirta et al., 2020; Molli et al., 2021). The North Apuane Fault, trending about NEE-SWW, is the most prominent structure of the linkage

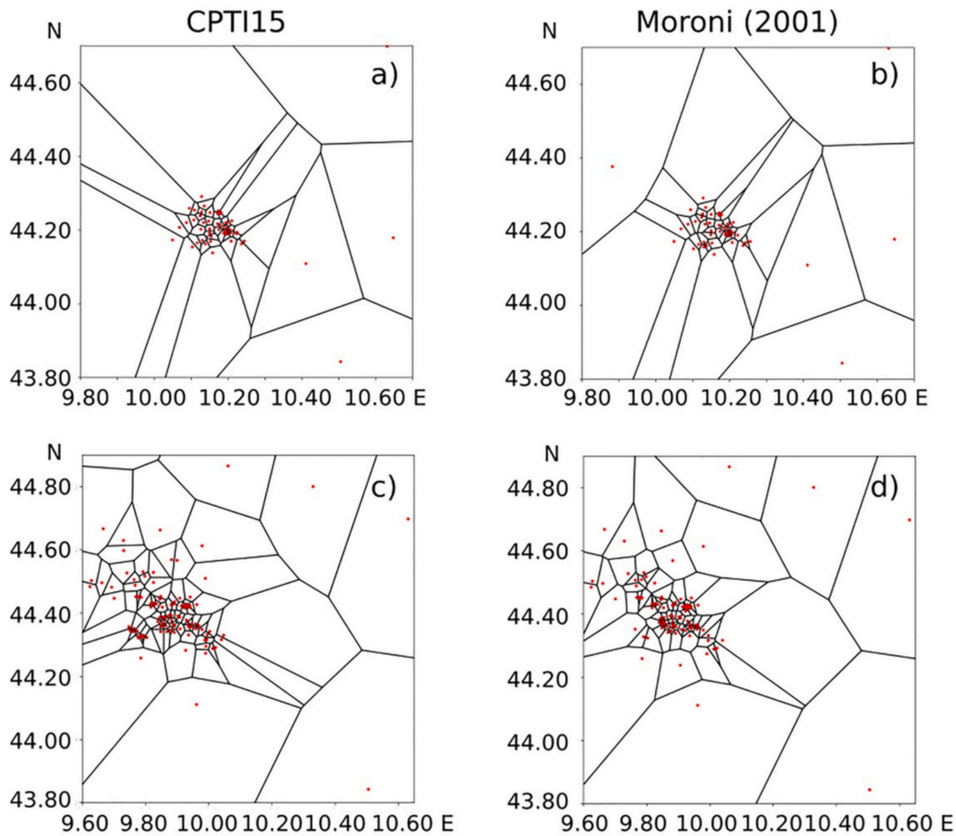

Fig. 5. the spatial distributions of the four datasets used in this work, tessellated by Voronoi polygons, are shown: a) earthquake of 11 April 1837 CPTI15; b) earthquake of 11 April 1837 Moroni (2001); c) earthquake of 14 February 1834 (CPTI15, Locati et al., 2022); d) earthquake of 14 February 1834 Moroni (2001). Voronoi polygons are convex surfaces where each point within the polygon is closer to the data site (which generates the polygon) than to any other data site (Okabe et al., 2000). In this way, the distribution and density of the data can be better detected. This method is useful to show qualitative data such as the macroseismic intensity (Pettenati et al., 1999).

system and is well constrained both at the surface and subsurface where it is well imaged down to ~5 km-depth. Dipping by about 50° toward N-NE, it separates a metamorphic footwall domain (Apuane metamorphic units in surface and subsurface) from the un-metamorphic cover units of the nappe stack (Molli et al., 2016; Molli et al., 2018). In the hanging wall of the main fault structure, the secondary splay faults are figured. As documented and discussed in Molli et al. (2018), the North Apuane Fault possibly reactivated in the extensional regime a previously-developed contractional lateral ramp.

The relocation of the main shock and aftershocks of the 2013 Lunigiana sequence clearly documents that the seismic activity is related to ruptures along the North Apuane Fault and its secondary splays. According to the KF results, we speculate that the North Apuane Fault may have caused the 1837 event as well and it represents an historical analogue of the later 2013 Lunigiana earthquake. The north dipping nodal plane of both earthquakes is compatible with the kinematics of such a fault; moreover, the location of the 1837 earthquake, although east of the 2013, is well consistent with the geometry of the fault (Fig. 7).

5.2. Cross-section 2

In cross-section 2 (Fig. 8) four different groups of units are distinguished:

- the Epiligurian, Ligurian and sub-Ligurian accretionary wedge units;
- the silici-clastic foredeep and the Plio-Quaternary fill of Pianura Padana;
- the Mesozoic mainly carbonates, cover of the proximal to distal Adria-plate;
- the *seismic basement* characterised by the seismic velocity of and higher than 5 Km/s.

The seismic basement was reached in the Pontremoli borehole (Lo Pò et al., 2016; Molli et al., 2018), and correlated in its westernmost part with the exposed Tuscan Metamorphic units and the underlying more external basement ones following Molli et al. (2018).

Three different structural and seismotectonic domains (Fig. 8) may be distinguished on the basis of: i) position of the Moho; ii) surface and subsurface structure; iii) kinematics of faulting: iv) depth of seismicity and relationships with the crustal-scale structures.

First order discontinuities of the two Moho's monoclines clearly define the domain 1 and 2 (Fig. 8): an external Adria-Moho showing a westward-dipping attitude from a depth of c.40 Km below the Po Plain down to c.50 Km depth below the NA chain in the domain 1 and an internal shallow "Thyrrhenian" Moho slightly deepening eastward from c.25 Km to c.30 Km depth border the domain 2. In between, a c. 10 km wide domain, which we name domain 3, east of the main orographic Apennines-divide, may be defined.

The easternmost external domain (domain 1 in Fig. 8) includes the buried ADF in the Parma recess (Cuffaro et al., 2010; Livani et al., 2018) and, at the surface, the ARF associated with the Salsomaggiore thrust (Artoni et al., 2004; Oppo et al., 2013; Picotti and Pazzaglia, 2007). This domain is characterised by the structures related with SW-dipping blind thrusts and related folds involving the Permo?-Triassic clastic deposits, the Jurassic-Cretaceous shallow to deep-water carbonates and Miocene-Pliocene foredeeps (Fantoni and Franciosi, 2010; Livani et al., 2023). The thrusts involve intra-cover decollements as well as the basement where a positive inversion of previous Mesozoic extensional faults may

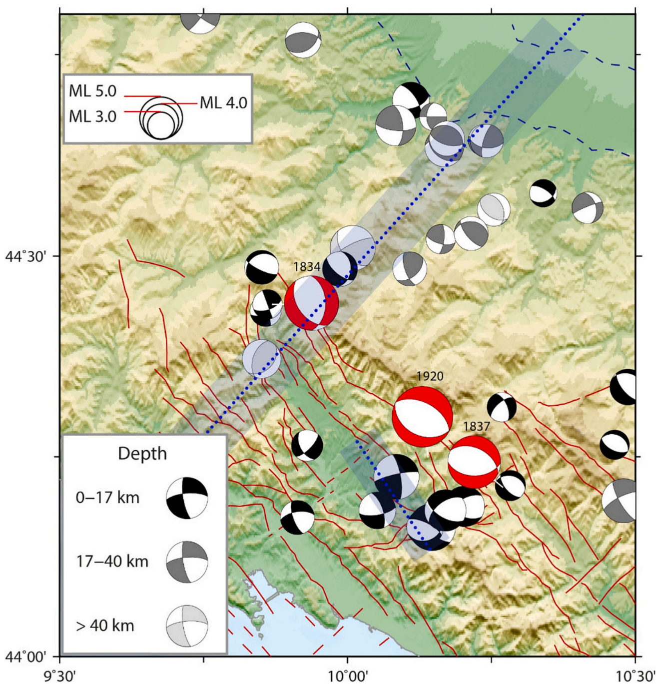

Fig. 6. Focal mechanisms for the area under study. In black and grey: focal solutions for the period 1995–2012 from Eva et al. (2014), 2012 to date computed for this study. In red: focal mechanisms of the historical earthquakes from the KF-NGA inversion (1834 and 1837). 1920 focal mechanism from Eva et al. (2022). (For interpretation of the references to colour in this figure legend, the reader is referred to the web version of this article.)

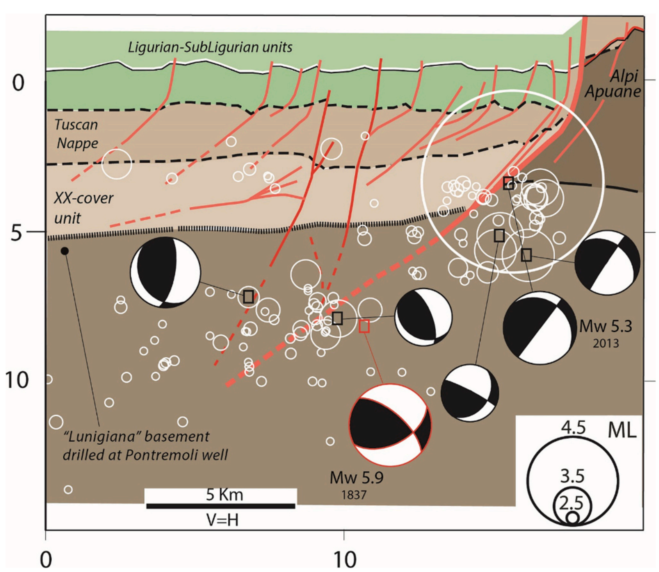

Fig. 7. Cross-section 1 across the NAF, transfer zone between Lunigiana and Garfagnana grabens. The cross-section is constrained in subsurface by the Eni S.p.A. seismic line (Camurri, 2000; Molli et al., 2016). In red the projected focal mechanism of the 1837 "Alpi Apuane" earthquake. It is important to underline that the appearance of focal mechanisms in section is different from those in plane view. In fact the focal mechanisms in section are visualized as the hemisphere vertically. (For interpretation of the references to colour in this figure legend, the reader is referred to the web version of this article.)

be suggested (Butler et al., 2004; Oppo et al., 2013; Turrini et al., 2016; Livani et al., 2018). In regards to the tectonic regime, an active contractional to transpressional kinematics is well documented by compressive focal solutions (Fig. 5), ranging from pure to oblique-slip mechanisms. Seismic events are mainly located deeper than 17 km depth although a small cluster of shallow events is also present, enlightening the superficial portion of thrusts on top of the carbonates and within the foredeep sediments.

The westernmost internal domain (domain 2), includes the Vara and Upper Lunigiana grabens and it extends eastward close to Apennines orographic divide. Dominant normal to oblique-slip faults shape this structural domain as previously illustrated. These fault systems have a geologically documented activity during Plio-Quaternary (Bernini and Papani, 2002; Brozzetti et al., 2007; Di Naccio et al., 2013; Nirta et al., 2020; Molli et al., 2021). Seismicity, shallower than c.12 Km depth, shows a connection with the mapped fault system at the surface. Moreover, a close relationship between the deepest seismicity and the subsurface trace of former contractional ramps in the basement suggests reactivations and negative inversion as dominant active structural processes.

Between domain 1 and domain 2 (see always Fig. 8), an intermediate shorter structural domain 3 may be recognized. It is characterised by the absence of normal faults at the surface and a clear structural signature connected with its present-day kinematics. The chain maintains its original contractional edifice as the dominant structural grain, however at depth an active extensional kinematics dominates. The normal EQ-faulting characterising this structural domain appears to be related with high amplitude and low-frequency reflective horizons interpreted as basement thrusts by Camurri (2000); Argnani et al. (2003) and Molli et al. (2018). The focal solution of Ml 3.4, 2006 earthquake and the associated seismicity suggest an ongoing normal-reactivation of the buried basement-thrust. In this same domain, according to the present study, within the accuracy of the KF computation, lies the 1834 "Pontremoli" earthquake, the focal solution of which is very similar to the 2006 event.

6. Discussion

The seismicity in the area under investigation is predominantly located northwest of the Alpi Apuane. Seismic events are scattered, bordering the Lunigiana graben, with dense clusters of epicentres marking the northern and southern terminations. The southern cluster, which encompasses the events of 2013, is oriented almost east-west and signifies the boundary between the Lunigiana and Garfagnana grabens. South of this cluster, there is a noticeable decrease in seismic activity, with a shift toward the eastern sector. The northern cluster, although less confined in size and number of events, conceals the prevailing apenninic NW-NNW orientation. To the northwest of the Lunigiana graben, seismic events align along an apenninic direction as well. On the outer side, earthquakes are nearly perpendicular to the chain in a NE-E orientation. South of the Parma valley, there is an aseismic area that extends to the border of the northern Garfagnana graben. A smaller aseismic area, bordered by two domains with anti-apenninic orientation, is located in the quadrant directly northwest of the 2013 events.

The comprehensive cross sections analysed in this study, where geological and seismic evidence are joined, confirm the complexity of this portion of the NW Apennines. We gain some help in interpreting the seismotectonics of the area from the focal mechanisms for historical earthquakes, namely the 1834 and 1837 events, achieved in the present study, and the 1920 earthquake, recently computed (Eva et al., 2022).

Concerning the apenninic seismicity, we propose that three domains are established along a NE/SW- oriented, two of them are well defined and "mature" (i.e. with correspondence between surface- subsurface structure and the current kinematics of faulting and related seismicity). In between the external and internal domain, an unripe "immature" extensional domain is evolving.

A partitioned East to West space- and depth-dependent kinematic frame is highlighted in agreement with the proposition of Eva et al. (2005). East of the orographic domain the buried fold and thrust system related with the ARF and the buried ADF is seismically active with its

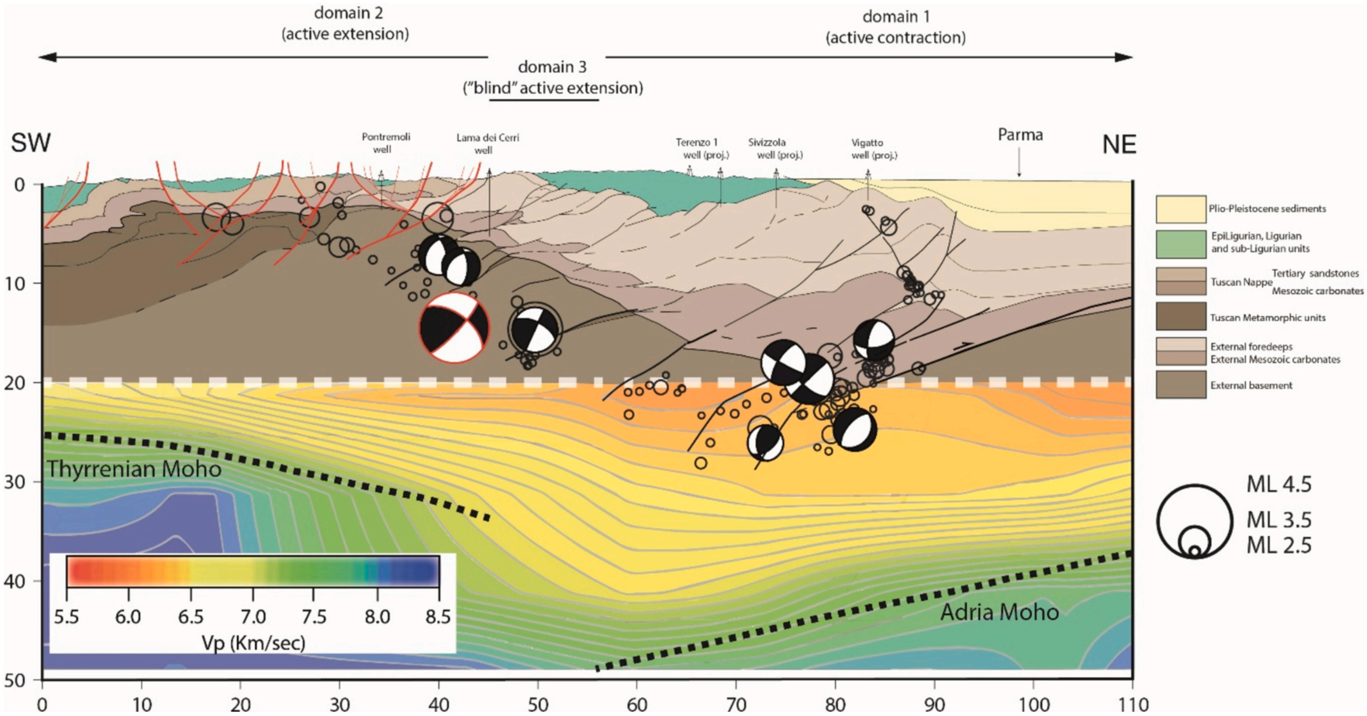

Fig. 8. Regional cross-section 2 based on subsurface data of Eni S.p.A. modified and reinterpreted after Camurri (2000); Camurri et al. (2001); Argnani et al. (2003); Carlini et al. (2013); Turrini et al. (2014); Martelli et al. (2016); Turrini et al. (2016); Livani et al. (2018) and Molli et al. (2018). The seismicity and focal mechanisms computed in this study are superimposed on the geological section. In red the focal mechanisms of the 1834 "Pontremoli" earthquake. In addition, the cross-section is completed at depth by the tomographic model by Scafidi and Solarino (2012). As in Fig. 7, the focal mechanisms in section are visualized as the hemisphere vertically. (For interpretation of the references to colour in this figure legend, the reader is referred to the web version of this article.)

basement-rooted thrusts and shallower subsurface splay faults. A contractional to inverse-slip kinematics characterises this domain. West of the orographic divide, steep NW-NNW trending high angle faults, combined in conjugated systems, are associated with an active extensional/transtensional kinematics. The seismicity in this westernmost domain is localised at shallow (max 12 Km) depth and roots in previously inherited contractional structures (basement ramps) and/or *syn*-contractional detachments (e.g. Molli et al., 2018). A shorter (c. 10 Km wide) active "buried" extensional domain shows the deepest extensional faulting as documented by focal mechanisms and appears to be as the easternmost toe of the extensional inner domain. We speculate that this domain, which we name domain 3 in Fig. 8, located on the vertical projection of the two opposite dipping Moho's ("Thyrrenian" vs "Adria"), may represent the active domain in which switching from shortening to extension is ongoing as an expression of the eastward mantle "nose" propagation (Chiarabba et al., 2014; D'Acquisto et al., 2020). This process involves energies that are sometimes released as major earthquakes, as witnessed by the 1834 event.

On the other hand, a second alignment of seismicity and related structures exists in the investigated area as in general throughout most of the Apennines. It is trending almost perpendicular to the dominant NW-SE and NNW-SSE and affects both the external easternmost domain as well as the internal westernmost domain.

In the internal domain, the seismicity is shallower than 10–12 Km. In the same domain, falls the area of the NAF system, the seismicity of which is shallow. The NAF acts as a transfer zone between Lunigiana and Garfagnana grabens (Brozzetti et al., 2007; Stramondo et al., 2014). This structure accommodates the different extension rate in the two grabens (Bennett et al., 2012; Molli et al., 2021) and it is the causative fault of the Mw 5.1, 2013 Lunigiana earthquake. According to our findings, this fault may be also related to the historical "Alpi Apuane"1837 earthquake.

In the external domain, the lateral ramp of the ADF, which defines the Parma recess, is associated with a medium to deep seismicity (deeper than 17 Km) as well as its buried equivalent structure vertically located below the Parma Valley. For these NE-oriented transverse structures, both in external as well as internal domains, a possible general relationship with segmentation of Adria lithosphere and tectonic inheritance from earlier stages of deformation (Royden et al., 1987; Doglioni et al., 1998; Faccenna et al., 2001) in turn controlled by paleogeographic heritage of the Adria-plate (Cuffaro et al., 2010; Turrini et al., 2016; Livani et al., 2018) may be envisaged.

7. Conclusions

The significance of the Lunigiana region in the study of northern Apennine seismotectonics is underscored by its recurrent and substantial seismic activity. This area has been the epicentre of several strong seismic occurrences, such as the Mw 6.5 earthquake in 1920, the Mw 5.6 event in 1481, and the Mw 5.9 earthquakes in 1834 and 1837. More recently, the area was affected by a Mw 5.1 earthquake in June 2013. Consequently, it is crucial to identify the geological structures that contribute to this seismic activity and to integrate them into the broader seismotectonic framework of the region to better assess their potential impact.

Our research indicates that the seismic activity within the study area is predominantly organized into clusters. The southern cluster is aligned in an approximately east-west direction and delineates the boundary between the Lunigiana and Garfagnana grabens, situated to the northwest of the Alpi Apuane. In contrast, the northern cluster exhibits a broader range in both size and frequency of seismic events, which obscures the prevailing NW-SE and NNW-SSE orientation characteristic of the Apennines. Additionally, to the northeast and west of the Lunigiana graben, seismic occurrences also align along an apenninic direction. On the external side, the earthquakes tend to be oriented nearly perpendicular to the mountain chain, displaying a NE-SW alignment. Geo-seismic cross-sections reveal the presence of three distinct domains along the northeast-southwest anti-apenninic axis. While the external and internal domains are clearly delineated, the intermediate domain may signify a transitional area where a shift from contractional to extensional tectonics is currently taking place, reflecting the eastward propagation of the Thyrrenian mantle. The tectonic processes within this domain can release significant energy, occasionally resulting in major seismic events, such as the earthquake recorded in 1834.

The comprehensive analysis conducted in this research, which encompasses instrumental seismicity, fault kinematics, structural architecture, and the focal mechanisms linked to both recent and historical earthquakes, yields a novel interpretation of the seismotectonics of this complex region. This, in turn, offers a new perspective on the historical earthquakes of the past two hundred years.

CRediT authorship contribution statement

E. Eva: Writing – review & editing, Writing – original draft, Visualization, Supervision, Investigation, Formal analysis, Conceptualization. **G. Molli:** Writing – review & editing, Writing – original draft, Visualization, Investigation, Conceptualization. **F. Pettenati:** Writing – review & editing, Writing – original draft, Visualization, Software. **S. Solarino:** Writing – review & editing, Writing – original draft, Supervision, Investigation, Formal analysis, Conceptualization.

Declaration of competing interest

The authors declare that they have no known competing financial interests or personal relationships that could have appeared to influence the work reported in this paper.

Data availability

Data will be available on request to the authors.

Acknowledgments

GM wants to acknowledge Andrea Artoni, Fabrizio Balsamo, Fabrizio Storti, Luigi Torelli and Paolo Vescovi for discussions and the sharing of data on the geology of the studied area.

FP thanks are due to Massimiliano Iurcev for the help in filling in some figures.

We are indebted to two anonymous reviewers who greatly contributed to the improvement of the manuscript.

References

Aki, K., Richards, G., G, P., 2002. Quantitative Seismology: Theory and Methods, 2° edition. W.HFreeman, San Francisco.

Argnani, A., Barbacini, G., Bernini, M., Camurri, F., Ghielmi, M., Papani, G., Rizzini, F., Rogledi, S., Torelli, L., 2003. Gravity tectonics driven by Quaternary uplift in the northern Apennines: insight from the La Spezia–Reggio Emilia geo-transect. Quat. Int. 101–102, 13–26.

Artoni, A., Papani, G., Rizzini, F., Calderoni, M., Bernini, M., Argnani, A., Roveri, M., Rossi, M., Rogledi, S., Gennari, R., 2004. The Salsomaggiore structure (northwestern Apennine foothills, Italy): A Messinian mountain front shaped by mass-wasting products. GeoActa 3, 107–127.

Benedetti, L., Tapponier, P., Gaudemer, Y., Manighetti, I., Van der Woerd, J., 2003. Geomorphic evidence for an emergent active thrust along the edge of Po Plain: the Boni-Stradella Fault. J. Geophys. Res. Space Physics 108, 2238. https://doi.org/10.1029/2001jb001546.

Bennett, R.A., Serpelloni, E., Hreinsdóttir, S., Brandon, M.T., Buble, G., Basic, T., Casale, G., Cavaliere, A., Anzidei, M., Marjonovic, M., Minelli, G., Molli, G., Montanari, A., 2012. Syn-convergent extension observed using the RETREAT GPS network, northern Apennines, Italy. J. Geophys. Res. 117, B04408. https://doi.org/10.1029/2011JB008744.

Bernard, P., Madariaga, R., 1984. A new asymptotic method for modeling of near-field accelerograms. Bull. Seismol. Soc. Am. 74, 539–5.

Bernini, M., Papani, G., 2002. Distensione della fossa tettonica della Lunigiana nordoccidentale (con carta geologica alla scala 1:50.000). Boll. Soc. Geol. Ital. 121, 313–341.

Bonini, M., Corti, G., Delle Donne, D., Sani, F., Piccardi, L., Vannucchi, G., Genco, R., Martelli, L., Ripepe, M., 2016. Seismic sources and stress transfer interaction among axial normal faults and external thrust fronts in the Northern Apennines (Italy): A working hypothesis based on the 1916–1920 time–space cluster of earthquakes. Tectonophysics 680, 67–89.

Brozzetti, F., Boncio, P., Di Naccio, D., Lavecchia, G., Tinari, D.P., Torelli, L., Bernini, M., Eva, E., Solarino, S., 2007. A multidisciplinary approach to the seismotectonics of the Lunigiana and Garfagnana extensional basins (Northern Tuscany, Italy). Rend. Soc. Geol. It. 5, 88–89.

Butler, R.W.H., Mazzoli, S., Corrado, S., De Donatis, M., Di Bucci, D., Gambini, R., Naso, G., Nicolai, C., Scrocca, D., Shiner, P., Zucconi, V., 2004. Applying thick-skinned tectonic models to the Apennine thrust belt of Italy—Limitations and implications. In: McClay, K.R. (Ed.), Thrust tectonics and hydrocarbon systems: AAPG Memoir, 82, pp. 647–667.

Camurri, F., 2000. Assetto stratigrafico strutturale delle unita' profonde di "basamento s. l." nell'Appennino settentrionale: dalla Val Ceno alla Valle del Reno, (PhD thesis, 117 pp.). University of Parma.

Camurri, F., Argnani, A., Bernini, M., Papani, G., Rogledi, S., Torelli, L., 2001. The basement of the North-Western Apennines: Interpretation of reflection seismics and geodynamics implications Fist (Federazione Italiana di Scienze della Terra). GEOITALIA 2001–31 Forum diScienze della Terra, Chieti, 5–8 Settembre 2001, Riassunti, pp. 50–51.

Carlini, M., Artoni, A., Aldega, L., Balestrieri, M.L., Corrado, S., Vescovi, P., Bernini, M., Torelli, L., 2013. Exhumation and reshaping of far-traveled/allochthonous tectonic units in mountain belts. New insights for the relationships between shortening and coeval extension in the western Northern Apennines (Italy). Tectonophysics 608, 267–287. https://doi.org/10.1016/j.tecto2013.09.029.

Carmignani, L., Kligfield, R., 1990. Crustal extension in the Northern Apennines: the transition from compression to extension in the Alpi Apuane core complex. Tectonics 9, 1275–1303.

Chiarabba, C., Giacomuzzi, G., Bianchi, I., Agostinetti, N.P., Park, J., 2014. From underplating to delamination-retreat in the northern Apennines. Earth Planet. Sci. Lett. 403, 108–116.

Cuffaro, M., Riguzzi, F., Scrocca, D., Antonioli, F., Carminati, E., Livani, M., Doglioni, C., 2010. On the geodynamics of the northern Adriatic plate. Rendiconti Fisiche Accademia di Lincei 21 (Suppl. 1), S253–S279. https://doi.org/10.1007/s12210-010-0098-9.

D'Acquisto, M., Dal Zilio, L., Molinari, I., Kissling, E., Gerya, T., van Dinther, Y., 2020. Tectonics and seismicity in the Northern Apennines driven by slab retreat and lithospheric delamination. Tectonophysics 789. https://doi.org/10.1016/j.tecto.2020.228481.

Devoti, R., Riguzzi, F., Cuffaro, M., Doglioni, C., 2008. GPS constraints on the kinematics of the Apennine subduction. Earth Planet Sc. Lett. 273 (163–174), 2008. https://doi.org/10.1016/j.epsl.2008.06.031.

Di Naccio, D., 2009. Morphotectonic analysis of the Lunigiana and Garfagnana Grabens (Northern Italy): Implications for Active and Potentially Seismogenic Normal Faulting. Università degli Studi di Chieti-Pescara. PhD thesis. 97 pp.

Di Naccio, D., Boncio, P., Brozzetti, F., Pazzaglia, F.J., Lavecchia, G., 2013. Morphotectonic analysis of the Lunigiana and Garfagnana grabens (northern Apennines, Italy): implications for active normal faulting. Geomorphology 201, 293–311.

Di Stefano, R., Ciaccio, M.G., 2014. The lithosphere and asthenosphere system in Italy as inferred from the Vp and Vs 3D velocity model and Moho map. J. Geodyn. 82, 16–25.

Di Stefano, R., Bianchi, I., Ciaccio, M.G., Carrara, G., Kissling, E., 2011. Three-dimensional Moho topography in Italy: New constraints from receiver functions and controlled source seismology. Geochem. Geophys. Geosyst. 12, Q09006. https://doi.org/10.1029/2011GC003649.

Diehl, T., Husen, S., Kissling, E., Deichmann, N., 2009. High-resolution 3-D P-wave model of the Alpine crust. Geophys. J. Int. 179 (2), 1133–1147. https://doi.org/10.1111/j.1365-246X.2009.04331.x.

Doglioni, C., Mongelli, F., Pialli, G., 1998. Boudinage of the Alpine belt in the Apenninic back-arc. Mem. Soc. Geol. Ital. 52, 457–468.

Elter, P., Giglia, G., Tongiorgi, M., Trevisan, L., 1975. Tensional and compressional areas in the recent (Tortonian to present) evolution of the Northern Apennines. Boll. Geofis. Teor. Appl. 17, 3–18.

Eva, C., Giglia, G., Graziano, F., Merlanti, F., 1978. Seismicity and its relation with surface structures in the North-Western Apennines. Boll. Geofis. Teor. Appl. 79, 263–277.

Eva, E., Ferretti, G., Solarino, S., 2005. Superposition of different stress orientations in the western sector of the northern Apennines (Italy). J. Seismol. 9, 413–430.

Eva, E., Solarino, S., Boncio, P., 2014. HypoDD relocated seismicity in northern Apennines (Italy) preceding the 2013 seismic unrest: seismotectonic implications for the Lunigiana-Garfagnana area. Boll. Geofis. Teor. Appl. 55 (4), 739–754.

Eva, E., Malusà, M.G., Solarino, S., 2020. Seismotectonics at the transition between opposite-dipping slabs (western Alpine region). Tectonics 39. https://doi.org/10.1029/2020TC006086 e2020TC006086.

Eva, E., Pettenati, F., Solarino, S., Sirovich, L., 2022. The focal mechanism of the 7 September 1920, Mw 6.5 earthquake: insights into the seismotectonics of the Lunigiana–Garfagnana area, Tuscany, Italy. Geophys. J. Int. 228, 1465–1477. https://doi.org/10.1093/gji/ggab411.

Eva, E., Malusà, M.G., Solarino, S., 2023. The 2021–2022 Genoa seismic sequences reveal distributed strike-slip deformation in the Alps-Apennines transition zone, NW Italy. Tectonophysics 868. https://doi.org/10.1016/j.tecto.2023.230101.

Faccenna, C., Becker, T.W., Lucente, F.P., Jolivet, L., Rossetti, F., 2001. History of subduction and back-arc extension in the Central Mediterranean. Geophys. J. Int. 145 (3), 809–820. https://doi.org/10.1046/j.0956-540x.2001.01435.x.

Fantoni, R., Franciosi, R., 2010. 2010 Tectono-sedimentary setting of the Po Plain and Adriatic foreland. Rend. Fis. Acc. Lincei 21 (Suppl. 1), S197–S209. https://doi.org/10.1007/s12210-010-0102-4.

Frechet, J., 1985. Sismogenèse et doublets sismiques, Thèse d'Etat, 207 pp. Univ. Sci. Technol. Médic, Grenoble.

Gentile, F., Pettenati, F., Sirovich, L., 2004. Validation of the automatic nonlinear source inversion of the U.S. Geological Survey intensities of the Whittier Narrows, 1987 earthquake. Bull. Seismol. Soc. Am. 94 (5), 1737–1747.

Got, J.-L., Frechet, J., Klein, F.W., 1994. Deep fault plane geometry inferred from multiplet relative relocation beneath the south flank of Kilauea. J. Geophys. Res. 99, 15,375–15,386.

Gueguen, E., Doglioni, C., Fernandez, M., 1997. On the post-25 Ma geodynamic evolution of the western Mediterranean. Tectonophysics 298, 259–269.

Handy, M.R., Schmid, S.M., Bousquet, R., Kissling, E., Bernoulli, D., 2010. Reconciling plate-tectonic reconstructions of alpine Tethys with the geological–geophysical record of spreading and subduction in the Alps. Earth Sci. Rev. 102 (3–4), 121–158. https://doi.org/10.1016/j.earscirev.2010.06.002.

Kissling, E., 1988. Geotomography with local earthquake data. Rev. Geophys. 26 (4), 659–698. https://doi.org/10.1029/RG026i004p00659.

Lahr, J.C., 1999. HYPOELLIPSE/VAX: A computer program for determining local earthquake hypocentral parameters, magnitude and first-motion pattern (Y2K Compliant Version), Version 1.0. U.S. Geological Survey, Open-File Report 99-23, On-Line Edition.

Le Breton, E., Handy, M., Molli, G., Ustaszewski, K., 2017. Post-20 Ma motion of the adriatic plate: new constraints from surrounding orogens and implications for crust-mantle decoupling. Tectonics. https://doi.org/10.1002/2016TC004443.

Livani, M., Scrocca, D., Arecco, P., Doglioni, C., 2018. Structural and stratigraphic control on salient and recess development along a thrust belt front: the Northern Apennines (Po Plain, Italy). J. Geophys. Res.-Sol. Ea. 123 (4360–4387), 2018. https://doi.org/10.1002/2017JB015235.

Livani, M., Petracchini, L., Benetatos, C., Marzano, F., Billi, A., Carminati, E., Doglioni, C., Petricca, P., Maffucci, R., Codegone, R., Rocca, V., Verga, F., Antoncecchi, I., 2023. Subsurface geological and geophysical data from the Po Plain and the northern Adriatic Sea (North Italy). Earth Syst. Sci. Data 15, 4261–4293. https://doi.org/10.5194/essd-15-4261-2023.

Lo Pò, D., Braga, R., Massonne, H.-J., Molli, G., Montanini, A., Theye, T., 2016. Fluid-induced breakdown of monazite in medium-grade metasedimentary rocks of the Pontremoli basement (northern Apennines, Italy). J. Metamorph. Geol. 34, 63–84.

Locati, M., Camassi, R., Rovida, A., Ercolani, E., Bernardini, F., Castelli, V., Caracciolo, C. H., Tertulliani, A., Rossi, A., Azzaro, R., D'Amico, S., Antonucci, A., 2022. Database Macrosismico Italiano (DBMI15), versione 4.0 [Data set]. Istituto Nazionale di Geofisica e Vulcanologia (INGV). https://doi.org/10.13127/dbmi/dbmi15.4.

Martelli, L., Bonini, M., Calabrese, L., Corti, G., Ercolessi, G., Molinari, F.C., Piccardi, L., Pondrelli, S., Sani, F., Severi, P., 2016. Carta sismotettonica della Regione Emilia Romagna e Aree limitrofe. Regione Emilia Romagna 91. https://ambiente.regione.emilia-romagna.it/it/geologia/.

Michelini, A., Lomax, A., 2004. The effect of velocity structure errors on double-difference earthquake location. Geophys. Res. Lett. 31, L09602. https://doi.org/10.1029/2004GL019682.

Molli, G., Torelli, L., Storti, F., 2016. The 2013 Lunigiana (Central Italy) earthquake: seismic source analysis from DInSar and seismological data and geodynamic implications for the northern Apennines: a discussion. Tectonophysics 668-669, 108–112.

Molli, G., Carlini, M., Vescovi, P., Artoni, A., Balsamo, F., Camurri, F., Clemenzi, L., Storti, F., Torelli, L., 2018. Neogene 3-D structural architecture of the north-west Apennines: the role of the low-angle normal faults and basement thrusts. Tectonics 37, 2165–2196. https://doi.org/10.1029/2018TC005057.

Molli, G., Manighetti, I., Bennett, R., Malavieille, J., Serpelloni, E., Storti, F., Giampietro, T., Bigot, A., Pinelli, G., Giacomelli, S., Lucca, A., Angeli, L., Porta, L., 2021. Active Fault Systems in the Inner Northwest Apennines, Italy: a Reappraisal one Century after the1920 Mw~6.5 Fivizzano Earthquake. Geosciences 11 (3), 139. https://doi.org/10.3390/geosciences11030139.

Moroni, A., 2001. Ricerche di fonti storiche per la compilazione del catalogo dei terremoti con repliche dell'Italia settentrionale; riorganizzazione delle informazioni storico-macrosismiche sui maggiori terremoti della Toscana e dell'Emilia Romagna. Rapporto tecnico, Istituto Nazionale di Geofisica e Vulcanologia (INGV), Milano, 68 pp.

Moroni, A., Bellettati, D., Chignola, E., Stucchi, M., 1993. The earthquakes of 1834 in the Northern Apennines. Ann. Geofis. 36 (1), 301–308.

Nirta, G., Vittori, E., Blumetti, A.M., Di Manna, P., Benvenuti, M., Montanari, D., Perini, M., Fiera, F., Moratti, G., Baglione, M., Piccardi, L., 2020. Geomorphological and paleoseismological evidence of capable faulting in the Northern Apennines (Italy): insights into active tectonics and seismic hazard of the Lunigiana basin. Geomorphology 374. https://doi.org/10.1016/j.geomorph.2020.107486.

Okabe, A.B., Boots, B., Sugihara, K., Chiu, S.N., 2000. Spatial Tessellation, Second ed. Wiley, Chichester. 671 pp.

Oppo, D., Capozzi, R., Picotti, V., 2013. A new model of the petroleum system in the Northern Apennines, Italy. Mar. Pet. Geol. 48, 57–76.

Pettenati, F., Sirovich, L., 2003. Test of source-parameter inversion of the U.S. Geological Survey intensities of the Whittier Narrows, 1987 earthquake. Bull. Seismol. Soc. Am. 93 (1), 47–60.

Pettenati, F., Sirovich, L., 2007. Validation of the Intensity-based Source Inversions of three Destructive California Earthquakes. Bull. Seismol. Soc. Am. 97 (5), 1587–1606. https://doi.org/10.1785/0120060169.

Pettenati, F., Sirovich, L., Cavallini, F., 1999. Objective Treatment and Synthesis of Macroseismic Intensity Fields using Tessellation. Bull. Seismol. Soc. Am. 89 (5), 1203–1213.

Pettenati, F., Sirovich, L., Bjerrum, L.W., 2017. Fault sources and kinematics of the 1897 Assam (M_W8.1) and the 1934 Nepal (M_S8.2) earthquakes retrieved by *KF*-NGA inversion and their seismotectonic implications. Bull. Seismol. Soc. Am. 107, 5, 2480–2489. https://doi.org/10.1785/0120160391.

Pettenati, F., Sirovich, L., Sandron, D., 2018. Modern techniques of treating damage pattern (intensity) to retrieve information on the 6 May 1976 M6.4 earthquake. Boll. Geofis. Teor. Appl. 59, 445–462. https://doi.org/10.4430/bgta0250.

Pezzo, G., Boncori, J.P.M., Atzori, S., Piccinini, D., Antonioli, A., Salvi, S., 2014. The 2013 Lunigiana (Central Italy) earthquake: Seismic source analysis from DInSAR and seismological data, and geodynamical implications for the northern Apennines. Tectonophysics 636, 315–324. https://doi.org/10.1016/j.tecto.2014.09.005.

Piccardi, L., Nirta, G., Montanari, D., Moratti, G., Blumetti, A.M., Di Manna, P., Vittori, E., Baglione, M., Fabbroni, P., 2019. Geological Setting and First Paleosismological Data on the Mulazzo Fault (Lunigiana Basin, Northern Tuscany). GNGTS-2019 Volume Abstract. Session-S1, pp. 108–112. www3.ogs.trieste.it/gngts/index.php/15-pagina-sessione-2019/75-2019-1-1.

Picotti, V., Pazzaglia, 2007. A new active tectonic model for the construction of the Northern Apennines mountain front near Bologna (Italy). J. Geophys. Res. 113, B08412. https://doi.org/10.1029/2007JB005307.

Raggi, G., 1985. Neotettonica ed evoluzione paleogeografica plio-pleistocenica del bacino del Fiume Magra. Mem. Soc. Geol. Ital. 30, 35–62.

Reasenberg, P., Oppenheimer, D.H., 1985. FPFIT, Fortran computer program for calculating and displaying earthquake fault-plane solutions. USGS Open File Rept, pp. 85–739.

Rovida, A., Locati, M., Camassi, R., Lolli, B., Gasperini, P., Antonucci, A., 2022. Catalogo Parametrico dei Terremoti Italiani (CPTI15), versione 4.0 [Data set]. Istituto Nazionale di Geofisica e Vulcanologia (INGV). https://doi.org/10.13127/cpti/cpti15.4.

Royden, L., Patacca, E., Scandone, P., 1987. Segmentation and configuration of subducted lithosphere in Italy: an important control on thrust-belt and foredeep-basin evolution. Geology 15, 714–717.

Scafidi, D., Solarino, S., 2012. Can local earthquake tomography settle the matter about subduction in the Northern and Central Apennines? Response from a new high resolution P velocity and Vp/Vs ratio 3-D model. Tectonophysics 554, 63–73.

Schaff, D., 2004. Optimizing Correlation Techniques for improved Earthquake Location. Bull. Seismol. Soc. Am. 94 (2), 705–721. https://doi.org/10.1785/0120020238.

Sirovich, L., 1996. A simple algorithm for tracing out synthetic isoseismals. Bull. Seismol. Soc. Am. 86, 1019–1027.

Sirovich, L., Pettenati, F., 2004. Source Inversion of Intensity patterns of Earthquakes; a Destructive shock of 1936 in Northeast Italy. J. Geophys. Res. 109 (B10309), 1–16. https://doi.org/10.1029/2003JB002919.

Sirovich, L., Pettenati, F., Chiaruttini, C., 2001. Test of Source-Parameter Inversion of Intensity Data. Nat. Hazards 24, 105–131.

Sirovich, L., Pettenati, F., Sandron, D., 2009. Source- and site-effects in the intensities of the M5.4 July 29, 2008. Earthquake in South Los Angeles. Seismol. Res. Lett. 80 (6), 936–945. https://doi.org/10.1785/gssrl.80.6.967.

Solarino, S., 2005. The role of instrumental versus macroseismic locations for earthquakes of the last century: a discussion based on the seismicity of the North-Western Apennines (Italy). Ann. Geophys. 48 (6), 923–936.

Solarino, S., Ferretti, G., Eva, C., 2002a. Seismicity of the Garfagnana-Lunigiana (Tuscany, Italy) as recorded by a network of semi-broad band instruments. J. Seismol. 6, 141–152.

Solarino, S., Ferretti, G., Eva, E., 2002b. Crustal structure of the Lunigiana-Garfagnana area (Tuscany, Italy): seismicity, fault plane solutions and seismic tomography. Boll. Geofis. Teor. Appl. 43, 221–238.

Spada, M., Bianchi, I., Kissling, E., Piana Agostinetti, N., Wiemer, S., 2013. Combining controlled-source seismology and receiver function information to derive 3-D Moho topography for Italy. Geophys. J. Int. 194 (2), 1050–1068.

Stramondo, S., Vannoli, P., Cannelli, V., Polcari, M., Melini., D., Samsonov, S., Moro, M., Bignami, C., Saroli, M., 2014. X- and C-band SAR surface displacement for the 2013 Lunigiana Earthquake (Northern Italy): a breached relay ramp? IEEE J-STARS 7 (7), 2746–2753.

Strollo, A., Cambaz, D., Clinton, J., Danecek, P., Evangelidis, C.P., Marmureanu, A., Ottem Oller, L., Pedersen, H., Sleeman, R., Stammler, K., Armbruster, D., Bienkowski, J., Boukouras, K., Evans, P., Fares, M., Neagoe, C., Heimers, S., Heinloo, A., Hoffmann, M., Kaestli, P., Lauciani, V., Michalek, J., Odon Muhire, E., Ozer, M., Palangeanu, L., Pardo, C., Quinteros, J., Quintiliani, M., Antonio Jara Salvador, J., Schaeffer, J., Schloemer, A., Triantafyllis, N., 2021. EIDA: the European Integrated Data Archive and Service Infrastructure within ORFEUS. Seismol. Res. Lett. 92 (3), 1788–1795. https://doi.org/10.1785/0220200413.

Turrini, C., Lacombe, O., Roure, F., 2014. Present-day 3D structural model of the Po Valley basin, northern Italy. Mar. Pet. Geol. 56, 266–289. https://doi.org/10.1016/j.marpetgeo.2014.02.006.

Turrini, C., Toscani, G., Lacombe, O., Roure, F., 2016. Influence of structural inheritance on foreland-foredeep system evolution: an example from the Po valley region (northern Italy). Mar. Pet. Geol. 77, 376–398.

Waldhauser, F., Ellsworth, W.L., 2000. A double-difference earthquake location algorithm: method and application to the northern Hayward fault. California. Bull. Seismol. Soc. Am. 90, 1353–1368.

Wells, D.L., Coppersmith, K.J., 1994. New empirical relationships among magnitude, rupture length, rupture width, rupture area, and surface displacement. Bull. Seismol. Soc. Am. 84, 974–1002.

Wolfe, C.J., 2002. On the mathematics of using difference operators to relocate earthquakes. Bull. Seismol. Soc. Am. 92 (8), 2879–2892. https://doi.org/10.1785/0120010189.